IJLAI Transactions on Science and Engineering (ISSN: 3006-3418) 2025, vol. 3, no. 3, pp: 37–44

Image Shadow Removal Based on Improved Generative Adversarial Network

Yuchang Si[1]

College of Artificial Intelligence, Shenyang Normal University
110034 Shenyang, China
Received August. 5, 2025; Revised and Accepted August. 18, 2025

Abstract. Traditional deep learning-based shadow removal methods often alter the pixels in non-shadow areas and fail to produce shadow removal results with natural boundary transitions. To solve this problem, we propose a novel multi-stage shadow removal framework based on Generative Adversarial Networks (GAN). Firstly, the multi-task-driven generator respectively generates the corresponding shadow mask and shadow mask for the input image through the shadow detection subnet and the mask generation subnet. Secondly, guided by the shadow mask and shadow mask, the full shadow module and the partial shadow module are respectively designed, and different types of shadows in the image are removed in stages. The sequential data from multiple sensors is used as the input of the time series generative adversarial network to generate sequence data with temporal dynamic characteristics; the data synthesized by the time series generative adversarial network is used to replace the noise input data in the gradient-penalized WGAN generative adversarial network, and the discriminator combines graph convolutional networks, long short-term memory networks and attention mechanisms to more effectively explore the spatio-temporal correlations of multi-source heterogeneous sensing data and enhance the discriminative ability for sequential data. Then, a new combined loss function was constructed based on the least squares loss to achieve better results. Compared with the latest deep learning shadow removal methods, on the selected dataset, the balance error rate of the proposed method decreases by approximately 4.39%, the structural similarity increased by approximately 0.44%, and the pixel root mean square error decreases by approximately 13.32%. The experimental results show that the shadow removal results obtained by this method have smoother boundary transitions.

Keywords: Deep learning, Generative Adversarial Network, Image processing, Shadow removal, Shadow detection.

1. Introduction

Shadows are widely present in images, and they can provide many important information for computer vision research tasks such as image depth estimation. However, they also significantly increase the difficulty of tasks such as object detection and target tracking [1]. Therefore, image shadow removal has always been a research hotspot in the field of image processing. Shadows have various shapes and types, and their types can be divided into full shadows and partial shadows: Full shadows are located within the shadow area, where the light source is completely blocked, and their brightness is relatively low and the color is darker. The penumbra lies between the umbra and the non-shadow area [2]. The illumination from the light source gradually returns to normal. Under the combined influence of ambient light and the light source, its brightness gradually increases and its color gradually returns to normal. The shadow removal method usually requires shadow positioning and shadow removal in sequence. During the shadow positioning process, the methods used in references [3,4] are shadow detection.

Reference [5] was based on the statistical learning method, but this method overly relied on custom shadow features. Reference [6] used a convolutional neural network (CNN) for shadow detection, but due to the limitations of the dataset size and the block processing mechanism, this method had poor generalization ability, and on the other hand, required additional global optimization steps to ensure the global coherence of the image. The artificial marking method used in references [7,8] could accurately locate shadows, but it required a large amount of additional annotation work. In the shadow removal process, traditional shadow removal methods can be classified into the illumination migration methods [9], the gradient domain removal methods [10], and the color domain removal methods [11]. In the references [12], the optimal non-shadow blocks for the shadowed image blocks were found using the illumination migration method, and then the illumination information was filled. However, due to the need for a series of preprocessing such as image segmentation and clustering, the efficiency needs to be improved. In the references [13], the gradient domain removal method merely altered the gradient variables of the halftone, and thus was not applicable to the illumination variables of the full image. In the color domain removal methods, in reference [14], the Bayesian formula was used to extract the mask image to remove the shadows in the image, while in reference [15], the intensity surface restoration method was used to remove the shadows.

In recent years, end-to-end shadow removal methods [16,17] have rapidly become the mainstream due to their high computational efficiency. These methods can be classified into eigenvalue decomposition methods [18] and deep learning methods [19]. In reference [20], the shadow detection step was bypassed through eigenvalue decomposition. However, this method altered the color of non-shadow areas, which gone against the original intention of shadow removal. Among the numerous shadow removal methods based on deep learning, the work [21] used CNN and combined the appearance and semantic information of shadows in the image to generate a mask for the shadow image, thereby obtaining the shadow removal result. Reference [22] employed two-condition generative adversarial networks (cGANs) to conduct shadow detection and shadow removal respectively. Reference [23] constructed a shadow image attenuator based on cGANs to generate diverse image samples, thereby enhancing the generalization ability of the model. Reference [24] used shadow images and their corresponding non-shadow images for supervised learning training. The data collection process involved using a camera to first capture shadow images, and then removing different shapes of obstructions to capture the corresponding non-shadow images. This type of method constructs a dataset with a significant problem: When capturing shadow images and their corresponding non-shadow images, due to changes in the camera exposure and posture, as well as the ambient lighting, the image pairs composed of the shadow images and the corresponding non-shadow images are inconsistent in terms of color information, lighting information, or spatial position. This will prevent the model from accurately learning the intrinsic relationship between shadows and non-shadows, thereby resulting in a phenomenon where the color and lighting information of the shadow recovery area and the non-shadow area are not coherent.

In order to achieve better shadow removal results, this paper first combines the multi-task learning method to conduct shadow detection and mask generation on shadow images. The shadow detection task aims to identify the positions of different types of shadows, while the mask generation task simulates the intrinsic relationship between shadow pixels and non-shadow pixels. On this basis, different modules are designed for different types of shadows to remove full shadows and partial shadows in a phased manner, so as to obtain a shadow removal result with natural boundary transitions.

2. Multi-stage Generative Adversarial Network

2.1. Time Series Generative Adversarial Network

TimeGAN consists of four networks: the embedding network, the recovery network, the sequence generator, and the sequence discriminator [25]. The core of the TimeGAN model lies in the joint training of the autoencoder network (embedding network and reconstruction network) and the adversarial network (sequence generator and sequence discriminator). This training mechanism enables TimeGAN to effectively capture the dynamic characteristics of data that change over time while learning to encode features and generate temporal sequence representations. The autoencoder network is trained through supervision and reconstruction losses, where the reconstruction loss ensures the accuracy of the learned latent representation, and the supervision loss guides the sequence generator to learn the temporal dynamic characteristics of the data. The embedding network and the recovery network establish a mapping relationship between the features and the latent space, allowing the adversarial network to learn the temporal dynamic characteristics of the data through low-dimensional representations. The formula of the embedding network is as follows:

$$h_s = e_s(s). \tag{1}$$

$$h_t = e_x(h_s, h_{t-1}, x_t). \tag{2}$$

Where s and x_t represent the static features and spatial features respectively. h_s and h_t are mapped into feature vectors in the latent space through the embedding function. The recovery network restores the static features r_s and temporal features r_x in the latent space to their initial states, as shown in the following formula.

$$\tilde{s} = r_s(h_s). \tag{3}$$

$$\tilde{x}_t = r_x(h_t). \tag{4}$$

The sequence generator uses random variables z_s and z_t to synthesize samples. By capturing the static features $\hat{h}_s$ and temporal features $\hat{h}_t$ in the latent space, it generates new features h_s and h_t.

$$h_s = g_s(z_s). \tag{5}$$

$$h_t = g_x(\hat{h}_s, \hat{h}_{t-1}, z_t). \tag{6}$$

The sequence discriminator is used to determine the authenticity of the data in the latent space. The formula is as follows:

$$\tilde{y}_s = d_s(\tilde{h}_s). \tag{7}$$

$$\tilde{y}_t = d_x(\overleftarrow{u}_t, \overrightarrow{u}_t). \tag{8}$$

Where d_s and d_x are the feature discriminators, serving as classification functions for static and temporal features respectively. $\tilde{y}_s$ and $\tilde{y}_t$ are respectively the discriminator labels. $\overrightarrow{u}_t = \overrightarrow{c}_x(\tilde{h}_s, \tilde{h}_t, \overrightarrow{u}_{t-1})$ and $\overleftarrow{u}_t = \overleftarrow{c}_x(\tilde{h}_s, \tilde{h}_t, \overleftarrow{u}_{t+1})$ respectively represent the sequences of the forward and backward hidden states. c_x is a recursive function.

TimeGAN consists of three loss functions: reconstruction loss LR, unsupervised loss LU, and supervised loss LS. The formulas are as follows:

$$LR = E_{S,X\ P_{data}(x,y)}[||s - \tilde{s}||_2 + \sum_t ||x_t - \tilde{x}_t||_2]. \tag{9}$$

$$LU = E_{S,X\ P_{data}}[\log y_s + \sum_t \log y_t]. \tag{10}$$

$$LS = E_{S,X\ P_{data}}[\sum_t ||h_t - g_x(h_s, h_{t-1}, z_t)||_2]. \tag{11}$$

The TimeGAN models constructed in the text all adopt GRU (Gated Recurrent Unit) network models to build each component. The model consists of an embedding network, a recovery network, a generator, a discriminator, and a supervision network. Except for the supervision network which uses a 2-layer hidden layer, the other networks all use a 3-layer hidden layer. Among them, the sequence generator extracts random vectors from the input two-dimensional Gaussian white noise, converts them into time vector features, and inputs them into the latent space. The sequence discriminator is responsible for extracting time features from the latent space and discriminating between true and false. The embedding network maps the original sequence data to the latent space, while the recovery network is responsible for restoring the output of the latent space to data with the original sequence features. The adversarial network generates new sequence data using the features in the latent space. The supervision mechanism guides the synthetic data to approach the real sequence data by predicting the continuous sequence.

The algorithm flow of the model is as follows: Firstly, the minority samples in the imbalanced fault dataset are preprocessed, including data normalization and the construction of multi-sensor sequence data using a sliding window, forming multiple two-dimensional data samples; Secondly, TimeGAN uses real sequence sample data and random noise data to generate time series feature samples; Then, WGAN-GP uses real sequence sample data and the data generated by TimeGAN to generate more high-quality and diverse time series feature data; Finally, the above data processing steps are repeated for each type of minority sample fault to expand the imbalanced samples, thereby constructing a balanced dataset for fault diagnosis.

2.2. Shadow Module

If the types of shadows are not distinguished and a uniform strategy is adopted to handle all types of shadows, it will result in obvious shadow boundaries in the final result, which will greatly affect the visual appeal of the image and the machine understanding process. Therefore, the semi-shadow module combines perceptual loss and uses high-level semantic information as a guide to simultaneously repair the shadow boundary area within a small range and achieve a friendly transition at the shadow boundary. The semi-shadow module aims to repair the semi-shadow mask $\hat{M}_p$, the corresponding image area, and its internal structure is shown in Figure 1.

In Figure 1, the input of the penumbra module is the shadow mask $\hat{M}$ and the full shadow removal image y'. According to the requirements of the penumbra module, the penumbra mask $\hat{M}_p$ is extracted. Based on the idea of image restoration, $\hat{M}_p$ is taken as the area to be repaired in the image y'. Just like the shadow detection subnet and the mask generation subnet, its function is relatively independent. It undergoes pre-training to enable the final overall network to converge better during training. Its network input consists of a three-channel y' and a single-channel $\hat{M}_p$, forming a four-channel image; its output is a three-channel shadow removal image. The pre-training objective function of the boundary reconstructive atom network is shown in equation (12).

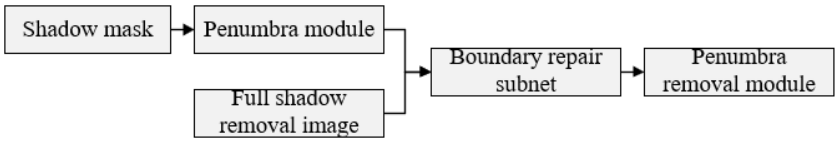

Fig. 1. Penumbra module

$$L_r = \frac{1}{N}\sum_{i=1} ||\hat{M}_p(y - R((1 - \hat{M}_p) \times y'))||^2. \tag{12}$$

Here N represents the number of training samples. y represents the label data of the real shadow-free image. $R(\cdot)$ is the output of the boundary reconstruction neural network. The boundary restoration sub-network aims to reduce the pixel differences between the restoration area and the GT image on the boundary semi-shadow area $\hat{M}_p$.

Inspired by the method in reference [26], if the model merely uses the pixel differences in equation (12) as the optimization objective, this pixel-based optimization approach will ignore the global similarity of the image, resulting in poor visual effects of the semi-shadow area in the shadow boundary restoration. This paper minimizes the differences in image semantics between the shadow-removed images and the real non-shadowed images by minimizing the perceptual loss function, as shown in equation (13). The key difference is that this paper no longer uses pre-trained deep networks to extract the features of the GT image and the shadow-removed image y', but instead uses the subsequent discriminator to extract the high-level semantic features of both, while significantly reducing the complexity of the model.

$$L_p = \sum_{i=1}^{n} \frac{1}{C_i H_i W_i} ||D_i(\hat{y}) - D_i(y)||^2. \tag{13}$$

Where n represents the total number of layers of the discriminator. $\hat{y}$ represents the shadow-free result obtained after being processed by the two modules in the past and the present. y represents the actual shadow-free image. D_i is the $i-th$ layer of the discriminator. C_i is the number of channels corresponding to the $i-th$ layer. H_i and W_i are the length and width of the feature map of the $i-th$ layer.

The discriminator in this paper is similar to that in reference [27]. The discriminator in this paper is designed to determine whether the shadow removal image generated by the generator for the shadow image is real. Essentially, this stage is an image binary classification problem. The discriminator consists of multiple convolutional blocks. In each convolutional block, the convolutional layer is immediately followed by batch normalization and Leaky Rectified Linear Unit (LReLU). The last layer of the discriminator is a Sigmoid function, whose output is the probability value that a pair of images is true.

2.3. Loss Function

The loss function of this network is mainly composed of the least mean square loss, supplemented by the average absolute error loss and the restoration loss, and its weighted form is as shown in equation (14). Its function is to perform final optimization towards additional constraints after the pre-training of multiple subnets. Therefore, its composition does not include the loss function term of pre-training.

$$L = \lambda_1 L_1 + \lambda_2 L_m + \lambda_3 L_p. \tag{14}$$

After analyzing the combination of loss functions, compared with the conventional adversarial loss function L_a, using the least mean square loss L_1 as the dominant one can yield better results, as shown in equation (15).

$$L_1 = E_{x,y-P_{data(x,y)}}[D(x,y)^2]. \tag{15}$$

Furthermore, the mean absolute error loss in equation (16) encourages the generated results to be closer to the true image without shadows.

$$L_m = \frac{1}{N}\sum_{i=1}^{N} ||y_i - \hat{y}_i||^2. \tag{16}$$

Here, N represents the number of training samples. Equation (16) is designed to obtain an average error.

3. Experiments and Result Analysis

3.1. Dataset

We combined the objective data sets SRD and ISTD into a comprehensive data set. Among them, SRD contains 3088 sets of shadow and non-shadow images, while ISTD contains 1870 sets of shadow, shadow binary masks, and non-shadow images. This paper uses the root mean square error (RMSE) of pixels to calculate the error between the shadow images and the real non-shadow images in the comprehensive dataset in the non-shadow areas. 1500 groups of images with less error and diverse scenes are selected. Then, the shadow images and non-shadow images in these 1500 groups of images are subtracted. Then, it subtracts the shadow images from the non-shadow images in these 1500 groups of images. We set the threshold at 20 in the three channels, and then perform morphological filtering and manually adjust the incorrect pixel labels of the shadow images to obtain the corresponding binary shadow masks for the dataset.

As shown in Figure 2, based on the binary mask of the shadows in the comprehensive screening dataset (Figure 2(b)), the shadow alpha mask is obtained using the image segmentation method in reference [28], as shown in Figure 2(b); using Equation (10), the sample mask in Figure 2(c) is obtained by dividing Figure 2(d) by Figure 2(a). Figures 2(a) and 2(b) are used for pre-training the shadow detection subnet, Figures 2(a) and 2(c) are used for pre-training the mask generation subnet, and Figures 2(a) and 2(d) are used to train the generator and discriminator in the network of this paper. Finally, 80% of the data in the comprehensive screening dataset is extracted for the training of the network of this paper, and the remaining 20% is used for feasibility verification.

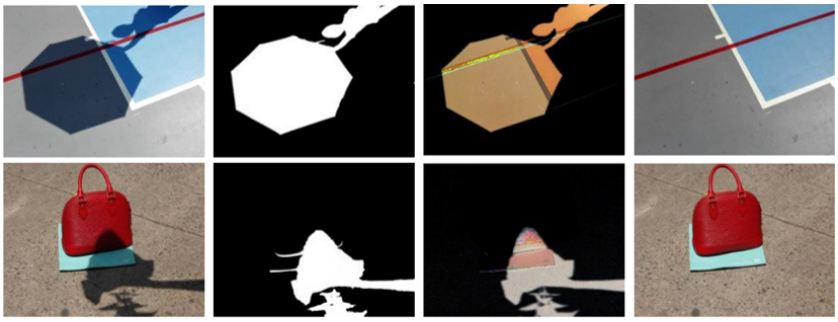

(a) Sample shadow image (b) Sample shadow mask (c) Sample mask (d) Sample image without shadow

Fig. 2. Samples of comprehensively filtered dataset

3.2. Objective Evaluation Indexes

Using the balanced error rate (BER) as the measurement index for shadow detection, the calculation method is as shown in equation (17).

$$BER = 1 - 0.5(\frac{TP}{TP+FN} + \frac{TN}{TN+FP}). \tag{17}$$

TP, TN, FP and FN represent the correctly generated negative image pixels, the correctly generated non-negative image pixels, the incorrectly generated negative image pixels, and the incorrectly generated non-negative image pixels respectively.

The RMSE and Structural Similarity Index (SSIM) are used as the measurement indicators for shadow removal. Among them, RMSE measures the error between the shadow-removed image and the true shadow-free image, while SSIM reflects the structural information and is more in line with human visual perception of the image.

$$RMSE = \sqrt{\frac{1}{n}\sum_{i=1}^{n}(I_i - I_i')^2}. \tag{18}$$

Here I and I' represent the images before and after shadow removal, composed of the R, G, and B color channels. n is the number of pixel points in the input image.

$$SSIM(x,y) = \frac{(2\mu_x\mu_y + c_1)(2\sigma_{xy} + c_2)}{(\mu_x^2 + \mu_y^2 + c_1)(\sigma_x^2 + \sigma_y^2 + c_2)}. \tag{19}$$

3.3. Results Quantification Analysis

Since shadow detection and shadow removal both belong to the relatively popular research directions in the field of image processing, and since many methods cannot simultaneously achieve both shadow detection and mask generation, this paper conducts experimental comparisons using images from different scenarios from the perspectives of shadow detection, mask generation, and the final shadow removal results.

Firstly, from the perspective of shadow detection, this paper analyzes the proposed method, DTN [29], and MAGC [30]. As shown in Figure 3, four images of different scenes are selected from the test set, including various types of shadows such as cross-texture shadows, soft shadows, and hard shadows to comprehensively test the detection performance of different methods. Specifically, DTN uses Support Vector Machine (SVM) to detect shadows, and then removes the shadows based on the physical lighting model. MAGC conducts shadow detection and shadow removal tasks simultaneously based on cGANs with shadow detection and shadow removal learning from each other and promoting each other.

Figure 3(a) shows the shadow image to be processed. Figure 3(b) shows the real shadow binary mask. Figure 3(c) shows the shadow detection result of DTN method. Figure 3(d) shows the shadow detection result of the MAGC method. Figure 3(f) shows the result of the method in this paper. Comparing Figure 3(b) and Figure 3(c), due to the lack of robust shadow features, traditional feature extraction machine learning methods cannot accurately detect the shallower shadows, such as the shadow of the umbrella on the cement ground in the second row and the shadow of the person on the grass in the fourth row. Compared with traditional machine learning methods, the MAGC method based on cGANs and this method perform relatively better in this aspect. Comparing Figure 3(d) and Figure 3(e), because this paper uses the Alpha Matting result as the training sample, the detection details at the shadow boundaries of this method are more abundant. Table 1 and table 2 are the specific objective evaluation indicators.

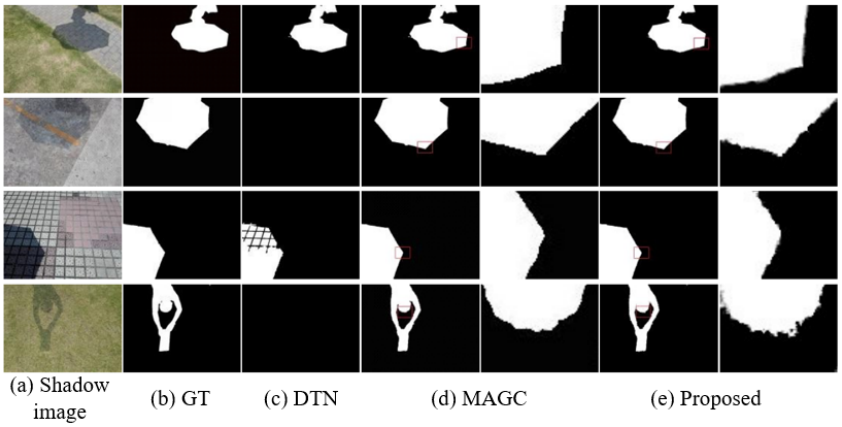

Fig. 3. Shadow detection results

Table 1. Results on SRD dataset with different methods

Method	RMSE	SSIM
DTN	7.12	0.9712
MAGC	6.65	0.9735
Proposed	5.45	0.9798

Table 2. Results on ISTD dataset with different methods

Method	RMSE	SSIM
DTN	8.05	0.9736
MAGC	7.47	0.9774
Proposed	6.68	0.9795

4. Conclusion

In order to obtain a shadow removal image with a smooth transition of shadow boundaries, a novel multi-stage removal method based on the generative adversarial network is proposed. The generator in this network has the ability of both shadow detection and shadow removal. The shadow detection subnet and the mask generation subnet provide accurate processing areas for the full shadow module and the semi-shadow module. Based on the idea of image restoration in small regions, combined with perceptual loss to reduce the differences in image semantics of the generated results, the transition of shadow boundaries will be more natural. In the future, the performance decline problem of deep learning methods when facing new datasets will be studied, and a domain transfer (Domain Shift) method for shadow removal will be implemented.

5. Conflict of Interest

The authors declare that there are no conflict of interests, we do not have any possible conflicts of interest.

Acknowledgments. None.

References

1. Sanin A, Sanderson C, Lovell B C. Shadow detection: A survey and comparative evaluation of recent methods[J]. Pattern recognition, 2012, 45(4): 1684-1695.
2. Shahtahmassebi A R, Yang N, Wang K, et al. Review of shadow detection and de-shadowing methods in remote sensing[J]. Chinese geographical science, 2013, 23(4): 403-420.
3. Khan S H, Bennamoun M, Sohel F, et al. Automatic shadow detection and removal from a single image[J]. IEEE transactions on pattern analysis and machine intelligence, 2015, 38(3): 431-446.
4. KaewTraKulPong P, Bowden R. An improved adaptive background mixture model for real-time tracking with shadow detection[M]//Video-based surveillance systems: Computer vision and distributed processing. Boston, MA: Springer US, 2002: 135-144.
5. Khan S H, Bennamoun M, Sohel F, et al. Automatic feature learning for robust shadow detection[C]//2014 IEEE conference on computer vision and pattern recognition. IEEE, 2014: 1939-1946.
6. Chai D, Newsam S, Zhang H K, et al. Cloud and cloud shadow detection in Landsat imagery based on deep convolutional neural networks[J]. Remote sensing of environment, 2019, 225: 307-316.
7. Shilpa M, Gopalakrishna M T, Naveena C. Approach for shadow detection and removal using machine learning techniques[J]. IET Image Processing, 2020, 14(13): 2998-3005.
8. Ding L, Zhang H, Xiao J, et al. A comprehensive approach for road marking detection and recognition[J]. Multimedia Tools and Applications, 2020, 79(23): 17193-17210.
9. Xiang J, Fan H, Liao H, et al. Moving object detection and shadow removing under changing illumination condition[J]. Mathematical problems in Engineering, 2014, 2014(1): 827461.
10. Jin Y, Sharma A, Tan R T. Dc-shadownet: Single-image hard and soft shadow removal using unsupervised domain-classifier guided network[C]//Proceedings of the IEEE/CVF international conference on computer vision. 2021: 5027-5036.
11. Khan S H, Bennamoun M, Sohel F, et al. Automatic shadow detection and removal from a single image[J]. IEEE transactions on pattern analysis and machine intelligence, 2015, 38(3): 431-446.
12. Zhang Z, Cao R, Sheng H, et al. Shadow detection and removal for remote sensing images via multi-feature adaptive optimization and geometry-aware illumination compensation[J]. Expert Systems with Applications, 2025: 127769.
13. Fan H, Han M, Li J. Image shadow removal using end-to-end deep convolutional neural networks[J]. Applied Sciences, 2019, 9(5): 1009.
14. Yuan D, Meng Y, Liu H, et al. An end-to-end shadow removal framework with an intuitive interaction scheme[J]. Pattern Recognition, 2026, 170: 112001.
15. Qu L, Tian J, He S, et al. Deshadownet: A multi-context embedding deep network for shadow removal[C]//Proceedings of the IEEE conference on computer vision and pattern recognition. 2017: 4067-4075.
16. Tang J, Luo Q, Guo F, et al. SDRNet: An end-to-end shadow detection and removal network[J]. Signal Processing: Image Communication, 2020, 84: 115832.

17. Le H, Samaras D. Shadow removal via shadow image decomposition[C]//Proceedings of the IEEE/CVF International Conference on Computer Vision. 2019: 8578-8587.
18. Gao J, Zheng Q, Guo Y. Towards real-world shadow removal with a shadow simulation method and a two-stage framework[C]//Proceedings of the IEEE/CVF Conference on Computer Vision and Pattern Recognition. 2022: 599-608.
19. Valanarasu J M J, Patel V M. Fine-context shadow detection using shadow removal[C]//Proceedings of the IEEE/CVF winter conference on applications of computer vision. 2023: 1705-1714.
20. Chen Z, Long C, Zhang L, et al. Canet: A context-aware network for shadow removal[C]//Proceedings of the IEEE/CVF international conference on computer vision. 2021: 4743-4752.
21. Lin Y F, Lee C M, Hsu C C. DenseSR: Image Shadow Removal as Dense Prediction[J]. arXiv preprint arXiv:2507.16472, 2025.
22. Guo L, Wang C, Wang Y, et al. Single-image shadow removal using deep learning: A comprehensive survey[J]. arXiv preprint arXiv:2407.08865, 2024.
23. Wang J, Li X, Yang J. Stacked conditional generative adversarial networks for jointly learning shadow detection and shadow removal[C]//Proceedings of the IEEE conference on computer vision and pattern recognition. 2018: 1788-1797.
24. Niu K, Liu Y, Wu E, et al. A boundary-aware network for shadow removal[J]. IEEE Transactions on Multimedia, 2022, 25: 6782-6793.
25. Zhang Y, Zhou Z, Liu J, et al. Data augmentation for improving heating load prediction of heating substation based on TimeGAN[J]. Energy, 2022, 260: 124919.
26. Liu Z G, Ji T Y, Chen J W, et al. Conditional-TimeGAN for realistic and high-quality appliance trajectories generation and data augmentation in nonintrusive load monitoring[J]. IEEE transactions on instrumentation and measurement, 2024, 73: 1-15.
27. Öztrk C. Enhancing Financial Time-Series Analysis with TimeGAN: A Novel Approach[C]//2024 9th International Conference on Computer Science and Engineering (UBMK). IEEE, 2024: 447-450.
28. Wang T, Zhang J, Zheng H, et al. MetaShadow: Object-Centered Shadow Detection, Removal, and Synthesis[C]//Proceedings of the Computer Vision and Pattern Recognition Conference. 2025: 28252-28262.
29. Wang X, Yao S, Tang Y, et al. Shadow-aware decomposed transformer network for shadow detection and removal[J]. Pattern Recognition, 2024, 156: 110771.
30. Zhang Z, Cao R, Sheng H, et al. Shadow detection and removal for remote sensing images via multi-feature adaptive optimization and geometry-aware illumination compensation[J]. Expert Systems with Applications, 2025: 127769.